Supporting information

Asymmetric ionic conditions generate large membrane curvatures

Marzieh Karimi[1], Jan Steinkühler[1], Debjit Roy[1,2], Raktim Dasgupta[1,3], Reinhard Lipowsky[1] and Rumiana Dimova[1]*

[1]Department of Theory and Bio-Systems, Max Planck Institute of Colloids and Interfaces, Science Park Golm, 14424 Potsdam, Germany

[2]Present address: Department of Cell Biology and Physiology, Washington University School of Medicine, St. Louis, Missouri 63110, USA

[3]Laser Biomedical Applications Section, Raja Ramanna Centre for Advanced Technology, 452013 Indore, India

*Address for correspondence: dimova@mpikg.mpg.de

Section S1. Preparation and observation of giant unilamellar vesicles (GUVs)

GUVs were prepared using the electroformation technique[1]. 2 mM solution of 1-palmitoyl-2-oleoyl-sn-glycero-3-phosphatidylcholine (POPC) containing a fraction (0.1 - 0.2 mol%) of 1,2-dioleoyl-*sn*-glycero-3-phosphoethanolamine-N-(cap biotinyl) in chloroform was prepared. Both lipids were purchased from Avanti Polar Lipids. Additionally, 0.1 mol% Texas Red 1,2-dihexadecanoyl-sn-glycero-3-phosphoethanolamine (Texas-Red-DHPE) or 0.2 mol% DiI ($DiIC_{18}(3)$; 1,1′-dioctadecyl-3,3,3′,3′-tetramethylindocarbocyanine, Thermo Fisher Scientific) was added for fluorescence imaging of the vesicles. Typically, 4 µl of the lipid solution was spread onto the electrically conductive side of indium tin oxide (ITO)-coated glass plates (Praezisions Glas & Optik, Iserlohn, Germany) and dried under vacuum for at least 30 minutes to remove the organic solvents. The amount of lipid solution was optimized for GUV yield to prevent vesicles attaching to each other. The glass plates were put against a 2 mm thick Teflon spacer to form a closed chamber held together by office clamps. The swelling solution (as indicated in the text) was added and a sinusoidal AC electric field at 10 Hz was applied for electro swelling of the lipid films. The voltage was held steady at 1.06 V_{rms} for 60 min. This voltage was measured at the ITO-coated glass plates. Once the vesicles were formed, they were diluted in the solution of interest (see main text) and transferred to the observation chambers to be used under the microscopes for further investigations. Both the drying and electro swelling were carried out at room temperature (23° C) at which the lipid bilayer is in the fluid phase. Vesicles were imaged using confocal microscope (SP5 DMI 6000, Leica Microsystems Heidelberg GmbH, Germany) or by the optical tweezers set up[2] built around a motorized inverted microscope (Axiovert 200M, Zeiss). For confocal imaging and statistics of vesicle morphologies, only vesicles with diameters larger than 15 µm were considered to correspond to the size range examined with micropipette manipulation and fluctuation analysis. The whole vesicle surface (and not only equatorial confocal cross sections) was explored for structures. The data in Table 1 in the main text is averaged over different vesicle preparations.

We also explored the response of individual vesicles subjected directly to exchange of the external solution. The GUVs labeled with 0.2 mol % DiI were prepared in 54 mM sucrose and observed under the epifluorescence microscope. The vesicles appeared spherical mostly without any internal or external structures. In the observation chamber, 50 µl GUVs suspension was directly diluted (20 times) with 30 mM LiCl solution to a final concentration 28 mM LiCl +2.7 mM sucrose outside the vesicles. Right after dilution, we tracked a vesicle to explore the morphological changes induced by the addition of LiCl. Figure S1 shows the formation of internal structures in the presence of LiCl implying the generation of negative spontaneous curvature.

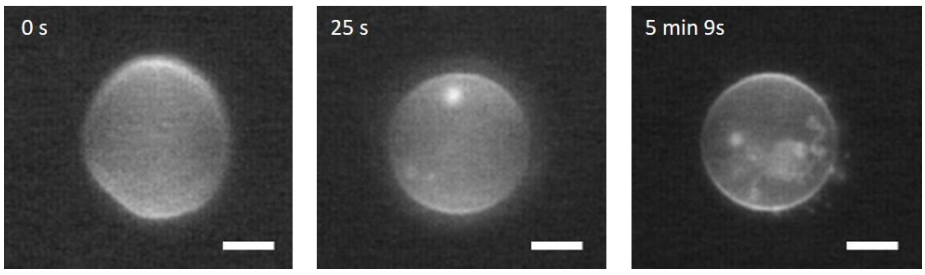

Figure S1: Epifluorescence images of one GUV prepared in 54 mM sucrose solution shortly after being exposed to LiCl solution of 28 mM final concentration in the chamber. The respective time stamps after starting the

observations (~10-20 seconds after having introduced the LiCl solution in the observation chamber) are indicated in the upper left corners of the images. With time, the vesicle develops internal tubes. Scale bar, 10 μm.

Section S2. Micropipette manipulation and aspiration of GUVs

Micromanipulation of GUVs was performed in a homemade experimental chamber. The chamber was built from two parallel 160 μm thick glass coverslips (24×50 mm^2 and 24×24 mm^2) separated by a U-shaped Teflon spacer with internal dimensions of 20 mm in width, length of 24 mm and height of 4 mm and an opening from one side in order to insert the micropipette to the chamber horizontally (Fig. S2). To deal with bead sedimentation in the chamber (beads then can stick to the bottom glass) and possible pollution of their surface by lipid aggregates floating in the solution, they were injected when needed via a needle in a hole on one side of the spacer using a syringe operated by a microinjector (model: IM-9B, Narishige Japan).

Micropipettes were pulled from borosilicate capillaries (1B100-4, World Precision Instruments Inc.) using a pipette puller (Sutter Instruments, Novato, CA) and then were cut using a microforge (Narishige, Tokyo, Japan) at desired inner diameters of ~7 μm. The adhesion of vesicle membranes to the pipette was prevented by incubation of the pipette tips in 5 mg/mL aqueous solution of BSA (Bovine Serum Albumin, Sigma Aldrich, Darmstadt, Germany). After the incubation, the micropipette was rinsed two or three times with the working solution in order to remove the BSA solution from the capillary tip. Moreover to prevent adhesion of the vesicles to the surfaces of the cover glass, the chamber was coated with 3-5 mg/mL ß-casein (Sigma) and then rinsed similarly with the experimental buffer. Additionally, the chamber was then prefilled with a solution containing GUVs for about 45 minutes and the solution discarded. In this way, areas not properly coated with casein were coated with membrane thus preventing adhesion and bursting of the fresh vesicles (which was often observed when working at high salt concentrations). This step also helped to remove the unbound ß-casein. Finally, we refilled the chamber with a fresh GUVs solution.

The chamber was mounted on the microscope and a single micropipette was inserted into the sample chamber using a three-dimensional micromanipulator system (Narishige Corp, Japan) clamped on the microscope (Fig. S2A). Equilibrium height of the water reservoir corresponding to zero pressure across the pipette tip was set when there was no flow of small particles in the vicinity of the tip. The aspiration pressure in the micropipette was controlled by changing the height of the reservoir mounted on a linear translational stage (M-531.PD; Physik Instrumente, Germany). The respective membrane tension Σ_{asp} was calculated from

$$\Sigma_{asp} = \Delta P \frac{R_{sp} R_{pip}}{2\left(R_{sp} - R_{pip}\right)}$$

where ΔP is the suction pressure, R_{sp} and R_{pip} are respectively the radii of the spherical vesicle and the micropipette. To apply the Laplace equation, the projection length of the vesicle must exceed the radius of the micropipette. Therefore we selected a well deflated vesicle and aspirated it with a high value of the aspiration pressure. This step of vesicle prestressing[3] ensured pulling out vesicle area stored in membrane folds and tubes. Then we decreased the pressure up to a point at which the micropipette could still hold the vesicle and the membrane tension was small. Few seconds after the attachment of a trapped bead to the vesicle, we slightly increased the distance between the bead and

vesicle membrane to attain a desired length of the tube (~10 µm). This length was kept constant during the whole experiment. Membrane tension was then increased slightly and for each tension the position of the bead relative to the trap center was recorded (500-1000 frames) by video microscopy. Note that it is important to set the zero reference pressure in the micropipette before each experiment on a new vesicle to compensate (small) changes in solution osmolarity by evaporation. This can be achieved by detecting the absence of a bead movement around the micropipette. All experiments were performed at room temperature, 23±1◦C.

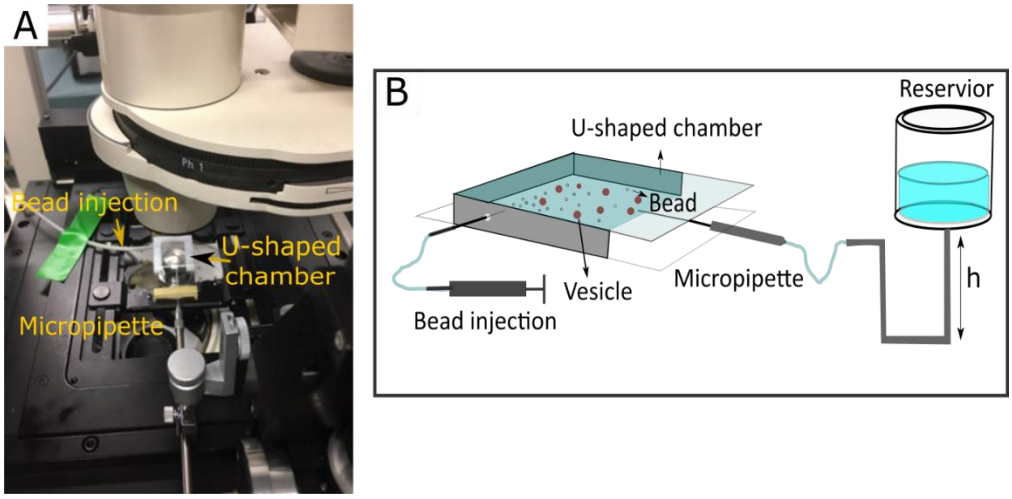

Figure S2: Observation chamber for micropipette manipulation. (A) A snapshot of the chamber at the microscope stage. (B) Schematic representation of the chamber and micropipette aspiration setup.

Section S3. Optical tweezers and force measurement

The optical tweezers was built around a motorized inverted microscope (Axiovert 200M, Zeiss) and a tightly focused laser beam from a 1064 nm continuous wave Nd:YAG laser (Spectra Physics, USA). Typical laser power used in our experiments was ~155 mW at the sample. Images were captured by an EMCCD camera (ImagEM, Hamamatsu Corp) at more than 40 frames per second. The optical tweezers was used to trap streptavidin-coated microspheres (Polyscience Inc., Cat #24160) with a diameter of ~1.9 µm. These microspheres can be attached to the biotinylated lipid membranes, which enables the manipulation of the vesicles in order to pull out tubes. When such tube is formed, the position of the bead is slightly displaced from the trap center. For small displacements, the force exerted by the tube is proportional to the bead displacement from the trap center. This force can be estimated by

$$f = -K(x - x_0) \tag{S1}$$

where $x - x_0$ is the displacement of the trapped bead from the trap center (x_0), when a tube is pulled and K is the trap stiffness. Quantitative use of the optical tweezers relies on accurate calibration of the trap stiffness which in our work is determined using the viscous drag method and the equipartition theorem (Section S4). In both methods, the bead was imaged using the EMCCD camera and its position was determined using centroid tracking algorithm[4] written in MATLAB (Mathworks Inc). All measurements were performed at a height of ~20 µm above the glass boundary of the sample chamber. The streptavidin-coated beads were washed to remove additives and residuals that

could interfere with the binding reactions of beads with GUVs. In this regard, the beads were spun down and washed three times using centrifuge at 13200 rpm for 3 min.

Section S4. Calibration of optical tweezers

When measuring tube pulling forces, the trapped bead was allowed to get displaced to the edge of the trap, i.e. away from the linear region of the trapping force field. This allowed us to assess higher forces (for the same trap beam power) than when using the linear trapping force region, resulting in reduced heating of the bead and attached vesicle. Moreover, considering possible variations of sizes of the trapped latex beads (see below) we calibrated the trap stiffness for each individual bead before using it for pulling tubes. An approach combining the equipartition theorem method and viscous drag method was used.

According to the equipartition theorem (ET), the trap stiffness is given by:

$$K_{ET} = \frac{k_B T}{\langle x^2 \rangle} \tag{S2}$$

where k_B is the Boltzmann constant, T is the absolute temperature and $\langle x^2 \rangle$ is the statistical variance in the trapped particle position resulting from the Brownian motion. Here, we consider only the trap stiffness in x-direction (the direction of tube pulling), which can be then used in Eq. S1 to obtain the force.

To record the particle and extract its displacement, we used an EMCCD camera with a pixel size of 154×154 nm^2 for the 100× objective lens used in our experiments. To determine the particle position, between 1000 and 2000 images of the bead were recorded (see Fig. S3) at acquisition speed of 47 frames per seconds. The position of the bead was determined using centroid tracking algorithm[4] written in MATLAB (Mathworks Inc). From the obtained bead trajectory (Fig. S3B) we could then determine the trap stiffness using Eq. S2.

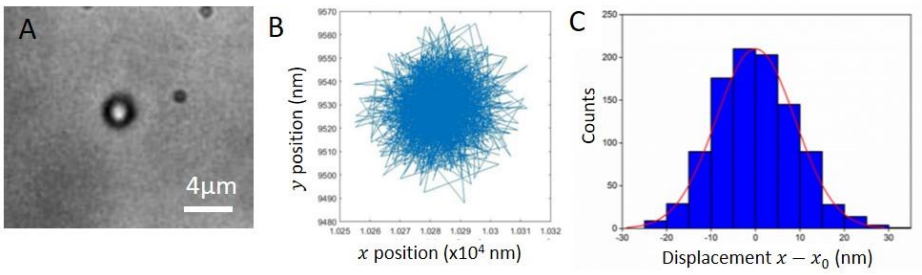

Figure S3. (A) Image of the trapped particle (142×128 pixels), (B) trajectory of the trapped particle recorded from 2000 images, and (C) a histogram of the particle displacement with a Gaussian fit (red curve). Here and in all other measurements, the laser power was set to that used in the tube-pulling experiments.

The camera exposure time and acquisition speed are important parameters affecting the position tracking of the trapped bead. At high exposure times, the position of the bead is averaged by the camera apparently increasing the trap stiffness, while at low exposure times, the noise in the image increases. The apparent trap stiffness measured using the equipartition theorem approach is shown in Fig. S4 for different values of the exposure time. A plateau region with no dependence of the trap stiffness on the exposure time was found for exposure times between 0.67 and 1 ms. Thus, in our experiments, the exposure time was set to be 0.86 ms. This exposure time was also corroborated by agreement between the viscous drag force method and the equipartition theorem approach as shown further.

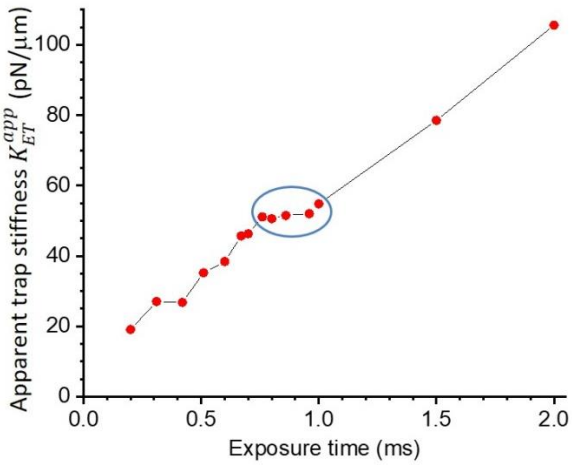

Figure S4. Apparent trap stiffness as a function of the camera exposure time. The data were obtained using the equipartition theorem approach. The plateau region is encircled.

Using the optimized exposure time and acquisition speed, we measured the trap stiffness using different beads (see red data points in Fig. S5). We observed deviations from particle to particle suggesting that the bead size/shape varied, presumably as a result from the streptavidin coating. This implied, that the trap stiffness calibration needs to be performed prior to tube pulling with the very bead used in the measurement.

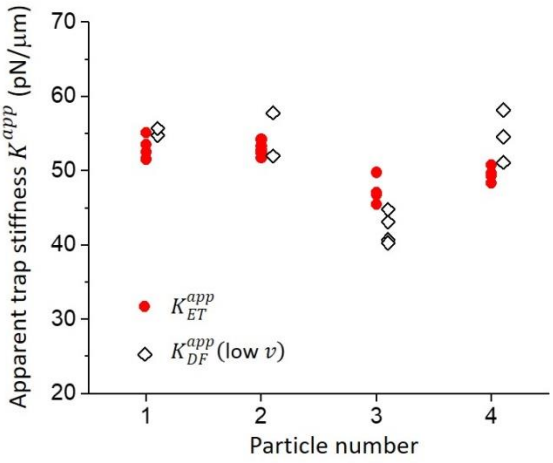

Figure S5. Apparent trap stiffness measured on different particles assessed from the equipartition theorem approach (red circles) and from the drag force at low stage velocity $\boldsymbol{v}$ = 0.5 mm/s (black diamonds), see text for details.

In the experiments when a tube was pulled, the trapped bead gets off-centered, i.e. the bead is located away from the equilibrium point in the focal plane because of the pulled tube. This results in a force different from that when the bead is near the center of the trap (as assessed with the equipartition theorem approach). To estimate the modified trapping force near the edge of the trap, we applied the viscous drag force (DF) method which is based on the application of a hydrodynamic force on the bead. This is implemented by moving the microscope stage. The force is described by the Stokes law:

$$F_{esc} = 6\pi\eta r v_{esc} \quad \text{(S3)}$$

where η is the viscosity of the solution, v_{esc} is the escape velocity (above which the particle leaves the trap) and r is the radius of the bead. The trap stiffness can be then determined from the escape force and the bead off-center displacement at velocity close to v_{esc}:

$$K_{DF} = \frac{F_{esc}}{x - x_0} \tag{S4}$$

It is pertinent to note here that measuring the escape force inside a vesicle suspension often results in losing the particle by collisions with surrounding vesicles as the stage has to be displaced at high velocity. To circumvent these difficulties, we developed the following approach. We measured an apparent trap stiffness (in vesicle free medium) for different stage velocities, v, defined as:

$$K_{DF}^{app}(v) = \frac{6\pi\eta r \Delta v}{\Delta(x - x_0)} \tag{S5}$$

where Δv sets the velocity range. Using Eq. S5, we determined the range of stage velocities, which yields apparent trap stiffness equal to that obtained with the equipartition theorem approach, $K_{ET}^{app} = K_{DF}^{app}(v)$, see Fig. S5. This range included low velocities between 0.2 and 0.8 mm/s.

As indicated above, in the tube-pulling experiments the bead is off-centered relocating to the periphery of the trap potential well because of the pulled tube. This significantly alters the force. We thus introduced a correction factor to account for this difference resulting from the off-centering. This correction factor is the ratio between the apparent trap forces measured at high and low stage velocities, $K_{DF}^{app}(\text{high } v)$ and $K_{DF}^{app}(\text{low } v)$, respectively. The range of high stage velocities corresponds to off-center displacement $x - x_0$ falling in the range of those measured during tube pulling. Figure S6 shows the off-center displacement in the two different velocity ranges. The slopes of the data yields $K_{DF}^{app}(\text{high } v)$ and $K_{DF}^{app}(\text{low } v)$.

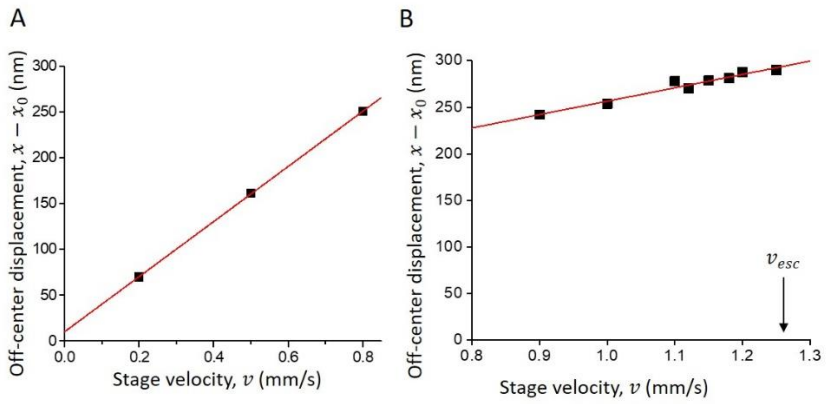

Figure S6. Bead off-center displacement $\boldsymbol{x - x_0}$ for (A) low and (B) high velocity of the stage. The two data sets were collected on the same bead. The slopes of the linear fits were used to determine $\boldsymbol{K_{DF}^{app}}(\text{low } \boldsymbol{v})$ and $\boldsymbol{K_{DF}^{app}}(\text{high } \boldsymbol{v})$, respectively.

Finally, the trap stiffness for each particle inside the vesicle suspension was estimated from measuring the apparent value from the equipartition theorem approach, K_{ET}^{app}, which was then corrected as follows:

$$K = K_{ET}^{app} \frac{K_{DF}^{app}(\text{high } v)}{K_{DF}^{app}(\text{low } v)} \quad \text{(S6)}$$

In our experiments the trap stiffness values were found to vary between 92.52 and 108.16 pN/μm for the different particles.

Section S5. Tube pulling experiment in high NaCl and KCl and vesicle leakage

In high salt concentrations, GUVs were grown in sucrose and then diluted in solutions of high concentrations of NaCl and KCl, separately. In these conditions, GUVs became very sticky to each other and some tubes were observed resulting from vesicle-vesicle adhesion and displacement. This could affect the pulling force if we used such vesicles interconnected with tubes. Besides the long tubes, we observed small outward protrusions which could be due to the adhesion of small vesicles and lipid patches to the GUVs. To work around this problem, we decreased the amount of lipid used to spread lipid on the ITO glasses while making GUVs. This decreased the possibility for vesicles contact. Moreover, in high asymmetry conditions, a few vesicles were found to have leaked as observed from their lower contrast. In this regard, we encapsulated 0.2 mol % of Rhodamine B (Sigma) in the GUVs prior to dilution in high salinity solutions. Figure S7A represents images of a vesicle containing Rhodamine B whereas Fig. S7B shows a vesicle which has lost its asymmetry and is not visible in epifluorescence microscopy. The lack of asymmetry in such vesicles does affect the spontaneous curvature. In this regard, we performed tube pulling experiment on two leaked vesicles and found that the lost asymmetry changes both the bending rigidity and the spontaneous curvature of vesicles to the values comparable to our results obtained at low NaCl asymmetry conditions (Fig. S7C and D). As shown in Fig. S7D, the loss of asymmetry leads to negligible spontaneous curvature, while vesicles with preserved asymmetry (intact) exhibit negative spontaneous curvatures. Similar results were obtained on leaked vesicles prepared with high KCl asymmetry (data not shown).

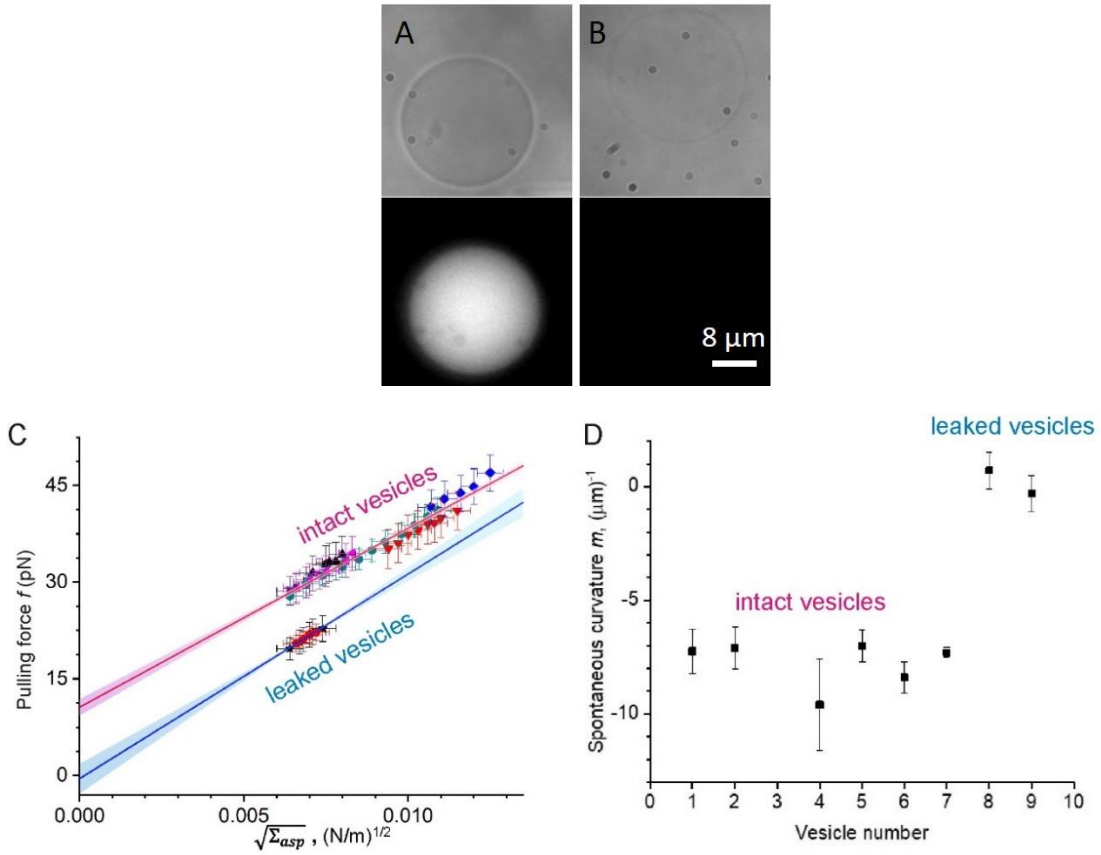

Figure S7. Imaging and measurements on intact and leaked vesicles prepared in the presence of Rhodamine B (encapsulated in their interior) and diluted in higly-concentrated NaCl solution corresponding to in high asymmetry of NaCl. (A, B) Bright field (upper panels) and apiflurescence images (lower panles) of GUVs. In one case, the vesicle has remained intact during the dilution step and is with preserved contrast (A), while in the other case, the vesicle has leaked and lost both contrast in bright field and in epifluorescence (B). (C) Tube pulling experiment on leaked and intact vesicles. (D) Data on the spontaneous curvature values in high NaCl asymmetry for intact and leaked vesicles.

Section S6. Mechanical properties of membrane under different asymmetry of sucrose and salt

The values of the bending rigidity and spontaneous curvature for each individual vesicle at different conditions are summarized in Tables S1-S5:

Table S1. The bending rigidity and spontaneous curvature for each individual vesicle exposed to low asymmetry of sucrose inside and NaCl outside the membrane.

Vesicle number	Bending rigidity (K_BT)	Spontaneous curvature (µm^{-1})
1	31.87±1.70	0.39±0.67
2	31.63±1.94	-0.26±1.10
3	33.57±1.28	0.79±0.50
4	32.84±1.63	-0.04±0.57
5	31.38±1.21	-0.43±0.58
Mean	32.25±1.55	0.09±0.68

Table S2. The bending rigidity and spontaneous curvature for each individual vesicle exposed to high asymmetry of sucrose inside and NaCl outside the membrane.

Vesicle number	Bending rigidity (K_BT)	Spontaneous curvature (μm^{-1})
1	27.49±2.43	-7.23±1.73
2	24.33±1.11	-7.15±1.12
3	23.74±2.16	-9.69±2.55
4	26.76±0.97	-7.03±0.71
5	24.57±3.16	-8.31±2.27
6	25.06±0.46	-7.47±0.38
Mean	25.32±1.71	-7.81±1.46

Table S3. The bending rigidity and spontaneous curvature for each individual vesicle exposed to low asymmetry of sucrose inside and KCl outside the membrane.

Vesicle number	Bending rigidity (K_BT)	Spontaneous curvature (μm^{-1})
1	34.06±0.31	-0.24±0.16
2	34.79±3.64	+0.45±1.70
Mean	34.42±1.9	0.12±1.35

Table S4. The bending rigidity and spontaneous curvature for each individual vesicle exposed to high asymmetry of sucrose inside and KCl outside the membrane.

Vesicle number	Bending rigidity (K_BT)	Spontaneous curvature (μm^{-1})
1	20.19±0.68	-10.64±0.34
2	26.52±1.84	-6.59±1.27
3	25.79±0.34	-6.44±0.26
4	24.57±0.82	-7.28±0.73
Mean	24.08±0.92	-7.73±0.65

Table S5. The bending rigidity and spontaneous curvature for each individual vesicle exposed to low asymmetry of sucrose inside and LiCl outside the membrane.

Vesicle number	Bending rigidity (K_BT)	Spontaneous curvature (μm^{-1})
1	17.37±0.46	-4.67±0.60
2	17.03±1.26	-5.05±1.62
3	18.85±0.77	-3.39±0.99
4	18.90±1.92	-2.73±2.09
Mean	18.03±1.09	-3.94±1.01

Section S7. Fluctuation analysis

The fluctuation analysis is based on collecting a time sequence of snapshots of the thermal fluctuations of the GUVs. Following the detailed description of this technique in [5], we measured the bending rigidity of the POPC vesicles which were exposed to different asymmetry conditions. The vesicle contours were precisely located in phase contrast images recorded using the fast digital camera HG-100K (Redlake Inc., San Diego, CA). Afterwards, the shape fluctuation analysis of the contours was performed to measure the bending rigidity[5]. We recorded a total of 5000 - 10000 snapshots per vesicle with exposure time of 200 μs and typical acquisition speed of 50 frames per second (fps). Only vesicles with clearly visible fluctuations and no visible defects were considered for analysis.

Section S8. Fluorescence lifetime measurements

In an attempt to resolve the nature of interaction of the different ions (suspected condensing effect of lithium ions versus depletion of sodium and potassium ions from the membrane), we performed fluorescence lifetime measurements of the membrane dye DiI. The fluorescence lifetime of this dye was previously shown to depend on the bilayer structure[6]. To this end, the GUVs were immersed in the high or low asymmetry salt buffers and the fluorescence lifetime of POPC GUV doped with 0.2 mol% of DiI was measured (ABBERIOR Instruments, 561 laser in pulsed mode). Fluorescence decays were fitted using SPCImage 5.3. Photon-counts were integrated over one quadrant of an individual GUV. If GUVs exhibited tubes or defects, only the segments of the smooth GUV membrane was considered. Fluorescent decays were fit using two-component exponentials and the weighted mean lifetime was reported. The instrument response function (IRF) was measured using DASPI dye dissolved in methanol. The IRF was then used to deconvolute the measurement data (parameters “shift” and “scatter” were fit using the SPCImage software). The lifetime measured for low and high NaCl and KCl asymmetry (as defined in Table 1 in the main text) were found similar and independent of salt concentration, see Fig. S8, with values close to literature data[6] for egg PC membranes (of which POPC is the major component). This suggests that no significant interaction in terms of intercalation in the membrane is observed for these salts and sugar. On the contrary, the lifetime distribution for the case of low LiCl asymmetry is significantly different ($p<0.05$) compared to the other monovalent salts, suggesting stronger interaction of the lithium ions with the membrane potentially implying intercalation or ion-induced lipid condensation.

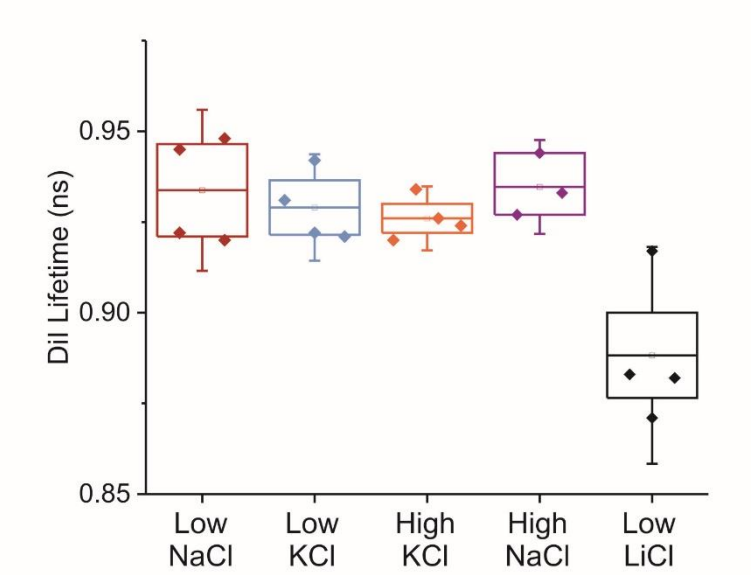

Figure S8. Fluorescence lifetime of DiI dye in the GUV membrane at varying solution asymmetry as defined in Table 1 in the main text.

References

1. Angelova, M. I.; Soléau, S.; Méléard, P.; Faucon, F.; Bothorel, P., Preparation of giant vesicles by external AC electric fields. Kinetics and applications. In *Trends Coll. Interf. Sci.*, Helm, C.; Lösche, M.; Möhwald, H., Eds. Steinkopff: 1992; Vol. 89, pp 127-131.
2. Kraikivski, P.; Pouligny, B.; Dimova, R., Implementing both short- and long-working-distance optical trappings into a commercial microscope. *Rev. Sci. Instrum.* **2006,** *77* (11), 113703.
3. Vitkova, V.; Genova, J.; Bivas, I., Permeability and the hidden area of lipid bilayers. *European Biophysics Journal with Biophysics Letters* **2004,** *33* (8), 706-714.
4. Dasgupta, R.; Verma, R. S.; Gupta, P. K., Microfluidic sorting with blinking optical traps. *Opt. Lett.* **2012,** *37* (10), 1739-1741.
5. Gracià, R. S.; Bezlyepkina, N.; Knorr, R. L.; Lipowsky, R.; Dimova, R., Effect of cholesterol on the rigidity of saturated and unsaturated membranes: fluctuation and electrodeformation analysis of giant vesicles. *Soft Matter* **2010,** *6* (7), 1472-1482.
6. Packard, B. S.; Wolf, D. E., Fluorescence lifetimes of carbocyanine lipid analogs in phospholipid bilayers. *Biochemistry* **1985,** *24* (19), 5176-5181.